IEEE International Workshop on Imaging Systems and Techniques (IST)

2022 IEEE International Conference on Imaging Systems and Techniques (IST)
DOI: 10.1109/IST55454.2022
21-23 June 2022

Showing 1-25 of 72

Proceedings

The proceedings of this conference will be available for purchase through Curran Associates.

Imaging Systems and Techniques (IST), 2022 IEEE International Conference on

- Print on Demand**Purchase at Partner**

Select All on Page

Sort By:

Enhanced Parasite Egg Images with Multiregion Light Source

Hsin-Yi Tsai;Yin-Ting Su;Yu-Hsuan Lin;Kuo-Cheng Huang;Chih-Ning Hsu;Ming-Li Liu

Publication Year: 2022,Page(s):1 - 5

- Abstract
- **HTML**
-
-

Detection of Face Features using Adapted Triplet Loss with Biased data

Sidra Bibi;Jitae Shin

Publication Year: 2022,Page(s):1 - 6

- Abstract
- **HTML**
-
-

HIHU-Net: A Hyper-Information Hybrid U-Net for Image Reconstruction with Electrical Impedance Tomography

Di Wang;Xinyu Zhang;Rong Fu;Zichen Wang;Xiaoyan Chen

Publication Year: 2022,Page(s):1 - 6

- Abstract
- **HTML**
-
-

Exploiting Mixed Reality in a Next-Generation IoT ecosystem of a construction site

Tina Katika;Fotios K. Konstantinidis;Thomas Papaioannou;Aris Dadoukis;Spyridon Nektarios Bolierakis;Georgios Tsimiklis;Angelos Amditis

Publication Year: 2022,Page(s):1 - 6

- Abstract
- **HTML**
-
-

A Sequence-selective Fine-grained Image Recognition Strategy Using Vision Transformer

Yulin Cai;Haoqian Wang;Xingzheng Wang

Publication Year: 2022,Page(s):1 - 6

- Abstract
- **HTML**
-
-

Ultrasound Image Segmentation for Deep Vein Thrombosis using Unet-CNN based on Denoising Filter

Moh Nur Shodiq;Eko Mulyanto Yuniarno;Johanes Nugroho;I Ketut Eddy Purnama

Publication Year: 2022,Page(s):1 - 6

- Abstract
- **HTML**
-
-

Two-stage Cascaded CNN Model for 3D Mitochondria EM Segmentation

Wei-Wen Hsu;Jing-Ming Guo;Jia-Hao Liu;Yao-Chung Chang

Publication Year: 2022,Page(s):1 - 5

- Abstract
- **HTML**
-
-

Development of a wide-field-of-view microscope objective system with high resolution and long working distance

Wei-Jei Peng;Chih-Wen Chen;Yi-Hao Lin;Ming-Fu Chen

Publication Year: 2022,Page(s):1 - 6

- Abstract
- **HTML**
-
-

Covid-19 Detection Based on Chest X-Ray Images Using DCT Compression and NN

Fatma Taher;Reem T Haweel;Usama Mohammad Hassan Al Bastaki;Eman Abdelwahed;Tariq Rehman;Tarek I Haweel

Publication Year: 2022,Page(s):1 - 5

- Abstract
- **HTML**
-
-

Aerial video inspection of Greek power lines structures using machine learning techniques

Aikaterini Tsellou;Konstantia Moirogiorgou;Georgios Plokamakis;George Livanos;Kostas Kalaitzakis;Michalis Zervakis

Publication Year: 2022,Page(s):1 - 6

Cited by: Papers (1)

- Abstract
- **HTML**
-
-

Machine Vision Based Granular Raw Material Adulteration Identification in Baijiu Brewing

Shanglin Yang;Yang Lin;Yong Li;Suyi Zhang;Lihui Peng;Defu Xu

Publication Year: 2022,Page(s):1 - 6

Cited by: Papers (1)

- Abstract
- **HTML**
-
-

Spectrogram Transformers for Audio Classification
Yixiao Zhang;Baihua Li;Hui Fang;Qinggang Meng
Publication Year: 2022,Page(s):1 - 6

- Abstract
- **HTML**
-
-

To Evaluate the Photo-activation Effect on Human Foot Under Near- or Far- Infrared Illumination by Using a Novel 2D Oxygen Saturation Image
Hsin-Yi Tsai;Yu-Hsuan Lin;Cheng-Ru Li;Kuo-Cheng Huang;Chun-Han Chou;Chih-Ting Lin
Publication Year: 2022,Page(s):1 - 6

- Abstract
- **HTML**
-
-

Smart Health Lighting Design Applied to Healthy Residential Environment
Ching-Ching Yang;Chun-Han Chou;Yin-Ting Su;Chen-Ru Lee;Yu-Hsuan Lin;Kuo-Cheng Huang
Publication Year: 2022,Page(s):1 - 6

- Abstract
- **HTML**
-
-

Design and validation of aberration-free plenoptic imaging system for industrial inspection
Chih-Hao Lin;Po-Ming Lin;Chih-Wen Chen;Ming-Fu Chen
Publication Year: 2022,Page(s):1 - 6

- Abstract
- **HTML**
-
-

AR Crew Rescue Assistant and AR Passenger Assistant Application for emergency scenarios on large passenger ships
Orestis Sampson;Spyros Bolierakis;Maria Krommyda;Lazaros Karagianidis;Angelos Amditis
Publication Year: 2022,Page(s):1 - 6

- Abstract
- **HTML**
-
-

I-PRIDe: Video-based Person Re-Identification
Jingwen Yang;Peter Leškovský;Andoni Cortes;Jorge García;Oihana Otaegui
Publication Year: 2022,Page(s):1 - 6

- Abstract
- **HTML**
-
-

Real-Time Object Detection using an Ultra-High-Resolution Camera on Embedded Systems
Marios Antonakakis;Aimilios Tzavaras;Konstantinos Tsakos;Emmanouil G. Spanakis;Vangelis Sakkalis;Michalis Zervakis;Euripides G.M. Petrakis
Publication Year: 2022,Page(s):1 - 6

- Abstract
- **HTML**
-
-

BUAS: A Knowledge-based Representation of the Border Surveillance Domain
Ioannis Kontopodis;Francisco Javier Iriarte;Peter Leškovský;Jorge García;Oihana Otaegui
Publication Year: 2022,Page(s):1 - 6

- Abstract
- **HTML**
-
-

Activation Function Selection for U-net Multi-structures Segmentation of End-Diastole and End-Systole Frames of Cine Cardiac MRI
Riandini;I Ketut Eddy Purnama;Eko Mulyanto Yuniarno;Mauridhi Hery Purnomo
Publication Year: 2022,Page(s):1 - 6

- Abstract
- **HTML**
-
-

Visualization of Flash Evaporation Process in Tiny Tube Based on Electrical Capacitance Tomography
Xiaolin Li;Jiangtao Sun;Peng Suo;Shiiie Sun;Lijun Xu
Publication Year: 2022,Page(s):1 - 6

- Abstract
- **HTML**
-
-

A Hybrid Qualitative-Quantitative Electromagnetic Imaging Method for Subsurface Prospecting
Valentina Schenone;Alessandro Fedeli;Matteo Pastorino;Andrea Randazzo;Claudio Estatico
Publication Year: 2022,Page(s):1 - 6

- Abstract
- **HTML**
-
-

Intelligent robotic system for urban waste recycling
Konstantia Moirogiorgou;Freiderikos Raptopoulos;George Livanos;Stavros Orfanoudakis;Maria Papadogiorgaki;Michalis Zervakis;Michail Maniadakis
Publication Year: 2022,Page(s):1 - 6
Cited by: Papers (1)

- Abstract

- **HTML**
-
-

Heatmap-based Explanation of YOLOv5 Object Detection with Layer-wise Relevance Propagation

Apostolos Karasmanoglou;Marios Antonakakis;Michalis Zervakis

Publication Year: 2022,Page(s):1 - 6

- Abstract
- **HTML**
-
-

Real-Time Hysteresis Foreground Detection in Video Captured by Moving Cameras

Hadi Ghahremannezhad;Hang Shi;Chengjun Liu

Publication Year: 2022,Page(s):1 - 6

- Abstract
- **HTML**
-
-
- 1
- 2
- 3
- >
-

IEEE Personal Account

- Change username/password

Purchase Details

- Payment Options
- View Purchased Documents

Profile Information

- Communications Preferences
- Profession and Education
- Technical interests

Need Help?

- US & Canada: +1 800 678 4333
- Worldwide: +1 732 981 0060
- Contact & Support

Follow

-
-
-

Ultrasound Image Segmentation for Deep Vein Thrombosis using Unet-CNN based on Denoising Filter

Moh Nur Shodiq
Dept. of Electrical Engineering
Institut Teknologi Sepuluh Nopember
Surabaya, Indonesia
Dept. of Informatic Engineering
Politeknik Negeri Banyuwangi
Banyuwangi, Indonesia
noer.shodiq@poliwangi.ac.id

Eko Mulyanto Yuniarno
Dept. of Electrical Engineering
Dept. of Computer Engineering
University Center of Excellence on Artificial Intelligence for Healthcare and Society (*UCE AIHeS*)
Institut Teknologi Sepuluh Nopember
Surabaya, Indonesia
ekomulyanto@ee.its.ac.id

Johanes Nugroho
Dept. of Cardiology
Universitas Airlangga
Surabaya, Indonesia
j.nugroho.eko@fk.unair.ac.id

I Ketut Eddy Purnama
Dept. of Electrical Engineering
Dept. of Computer Engineering
University Center of Excellence on Artificial Intelligence for Healthcare and Society (*UCE AIHeS*)
Institut Teknologi Sepuluh Nopember
Surabaya, Indonesia
ketut@te.its.ac.id

2022 IEEE International Conference on Imaging Systems and Techniques (IST) | 978-1-6654-8102-1/22/$31.00 ©2022 IEEE | DOI: 10.1109/IST55454.2022.9827731

***Abstract*— Deep vein thrombosis (DVT) is caused by an abnormal blood clot condition in the network of blood vessels. Several risk factors that often cause DVT are advanced age, post-surgery, hospitalization, pregnant women, and obesity. In general, Diagnosis of DVT uses ultrasound images. However, diagnosis using ultrasound manually takes a long time, and the accuracy of image reading depends on medical personnel. It requires a system that can detect DVT automatically. Also, it can be obtained quickly and has good accuracy. This study proposes a segmentation model for ultrasound images of deep vein thrombosis using U-Net CNN based on a denoising filter. Furthermore, calculating the suspected area to be DVT predicted using U-Net CNN. The denoising filter consisted of eight filters. That model system was tested with an ultrasound image dataset. The dataset was obtained from four volunteers. The volunteers have been identified as having symptoms of deep vein thrombosis. The dataset was captured and recorded using an ultrasound device carried out by medical experts. Each DVT recorded dataset is extracted into frames. The full frames obtained are 317 frames. Then the ultrasound image data is manually labeled by medical personnel. The experimental results show that the Gaussian filter has the best results, with 99% of accuracy and 0.0252 scores of an average loss parameter. Meanwhile, the DVT prediction test using U-Net CNN segmentation based on the calculation of the mean IoU is 84.9% accurate. The measure of the mean Hausdorff distance is 4.17 of the score. We want to investigate the detection and classification of DVT for further research.**

Keywords*— deep vein thrombosis, segmentation, Unet-CNN, denoising filter, ultrasound image

I. INTRODUCTION (*HEADING 1*)

Deep vein thrombosis (DVT) is caused by an abnormal blood clot condition in the network of blood vessels. Several risk factors that often cause DVT are advanced age, post-surgery, hospitalization, pregnant women and obesity [1]. This is still a health problem that continues to increase in the community. Based on data in the United States, it is estimated that there are 300,000 - 600,000 people experiencing symptoms of DVT / pulmonary embolism (PE). Research estimates that 10% - 30% of patients with DVT die within 30 days, while it is estimated that 20% - 25% of patients with PE experience sudden death [1].

Ultrasonography (USG) is still the standard for diagnostic imaging for patients with suspected DVT. Some use grayscale and use Doppler frequency. The currently recommended protocol is a full examination from the thigh to the ankle, applying Doppler ultrasound to specific areas. With Doppler, ultrasound can show the movement of material in the body, such as the movement of blood flow, so if there are abnormalities in the blood flow, DVT is suspected. The symptom area should be evaluated whether there is thrombosis in the deep vein or not [2]. However, manual ultrasound still takes a long time to diagnose, the accuracy of the diagnosis is limited due to wrong readings, and the experience of medical personnel influences subjective results. Thus, this requires a system that can detect the presence of DVT automatically, quickly and has good accuracy, and can also provide information on the estimated area of blood clots through ultrasound images. Implementing deep learning for autonomously detecting DVT will offer more benefits for medical personnel.

Previous research has been conducted by Chen Huang, et al. This study aims to segment DVT using a convolutional neural network. Dataset used in this research is Magnetic Resonance Image (MRI). However, using MRI images requires great effort because it relatively more expensive than ultrasound images [3]. Another related research has been carried out by Bernhard Kainz et al. This study diagnoses DVT using the U-Net convolutional neural network (CNN) architecture. U-Net CNN has been used for automatic segmentation of DVT areas. Dataset used is an ultrasound image. In general, ultrasound images do have not visually clear characteristics and contain noise speckle.

However, this study did not explain the enhancement of the denoising filter [4].

This research implements deep learning for segmentation autonomously using U-Net convolutional neural network (CNN) architecture. Firstly, the ultrasound image dataset is acquired and divided into three parts: learning data, evaluation data, and test data. Secondly, image enhancement process is done by using eight denoising filters. Third, Segmentation that uses the U-Net CNN architecture is processed. Finally, segmentation performance is tested by comparing the ground truth image with the predicted masking image.

II. Materials and Method

Ultrasound image segmentation using U-Net CNN for deep vein thrombosis using denoising filter in this research uses several steps: data acquisition, preprocessing model, segmentation method using U-Net CNN architecture, and segmentation performance metrics. The design of this system can be seen in Figure 1.

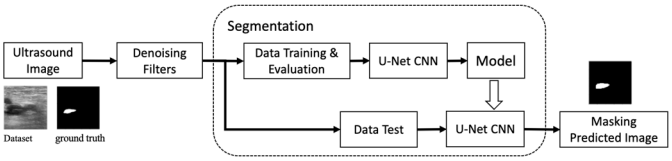

Fig. 1. System Design for DVT Segmentation using U-Net CNN based on Denosing Filter

A. Data acquisition

The DVT ultrasound dataset was obtained from four volunteers. The patient has been identified as having symptoms of deep vein thrombosis. Dataset was captured and recorded using ultrasound equipment performed by professional medical experts. Each DVT recorded video data was extracted into frames. The full frames obtained were 317 frames. Then, the ultrasound image data was manually labeled by a medical professional. The label data was used to develop a segmentation model using U-Net CNN. The dataset was divided into two parts, including training data and testing data. The number of datasets for training data was 80%, and evaluation data was 20%. It was determined randomly.

B. Preprocessing model

Preprocessing model aims to improve image quality, reduce noise, and preserve edges [5]. This process is required for B-mode ultrasound images because these images have characteristics that are not visually clear and contain a lot of noise speckle [6].

A denoising filter is a method for reducing noise in ultrasound images. The noise that appears on the ultrasound image is a speckle noise type. Many researchers have implemented a denoising filter in the preprocessing stage of medical image processing. In this study, several filters were implemented, including the wiener filter, Lee filter, non-local mean filter, median filter, Total variation filter, anisotropic diffusion filter, Gaussian filter, and wavelet filter. These filters were used for denoising the noise speckle in the ultrasound image. In this study the performance of the filter model was tested using deep vein thrombosis data. The detail of the denoising filter will be explained as follows.

1. Wiener Filtering

The Wiener filter reduces noise in ultrasound images based on the mean square error. Thus, this filter is the least mean square filter [7]. The Wiener filter is classical filtering that is included in multiscale filtering [8]. The equation of the Wiener filter as-is:

$$F(u,v) = \left\{ \frac{H(u,v)}{H(u,v)^2 + [S_n(u,v)/S_f(u,v)]} \right\} G(u,v) \tag{1}$$

where, $H(u,v)$ is the blurring filter or degradation function, $S_n(u,v)$ is the noise additive spectrum, $S_f(u,v)$ is the power spectra in the original image, and $G(u,v)$ Represents image that is degraded by noise.

2. Lee Filtering

Lee filter equation for denoising ultrasound image can be seen in the following formula [7].

$$Y(i,j) = I_m + W\left(C_p - I_m\right) \tag{2}$$

where, $Y(i,j)$ is the denoising speckle image, I_m denotes the mean of the kernel or window, C_p is the center element of pixel in the kernel, and W is a window. Meanwhile, W can be obtained by the following equation.

$$W = \frac{\sigma^2}{(\sigma^2 + \rho^2)} \tag{3}$$

where, $\sigma^2$is a variance of a pixel in the reference image, ρ^2 is variance of pixel in the noised speckle image. Meanwhile, to find $\sigma^2$and ρ^2 through the following equation.

$$\sigma^2 = \left[\frac{1}{m}\sum_{i=0}^{m-1}(X_i)^2\right] \tag{4}$$

$$\rho^2 = \left[\frac{1}{n}\sum_{j=0}^{n-1}(Y_i)^2\right] \tag{5}$$

where n and X_i is size of filter kernel and pixel value within the filter kernel. m is size of an image. Y_i is a pixel value of image.

3. Non-local means Filtering

Non-local filter is non-linier filter. This filter has been implemented to reduce speckle noise in carotid artery ultrasound images [9]. In addition to image filters, it can preserve the edges and details of the original images [10]. The non-local mean filter equation is as follows.

$$NL(u)(x_i) = \sum_{x_j \in \Omega^{dim}} w\left(x_i, x_j\right) u\left(x_j\right) \tag{6}$$

where, $NL(u)(x_i)$ is the restored intensity of pixel x_i, $w\left(x_i, x_j\right)$ is the weight assigned for restoring $u\left(x_j\right)$. Equation to find $w\left(x_i, x_j\right)$ is as follows.

$$w(x_i, x_j) = \frac{1}{Z_i} exp - \frac{\left\| u(\mathcal{N}_i - u(\mathcal{N}_j)) \right\|_{2,a}^2}{h^2} \quad (7)$$

Where, Z_i is the normalization constant and ensuring that $\sum_{x_j \in \Omega^{dim}} w(x_i, x_j) = 1$, while h acts as a smoothing parameter.

4. Median Filtering

The median filter is effective non-linear filtering. The median filtering method is simple. The median filter operation replaces the center pixel value with the median value of its neighbors [7].

5. Total Variation Filter

Total variation filter is useful for or recovering piecewise constant signals [11]. This filter can reduce noise and is able to keep the image from being distorted. The equation for the total variation filter is as follows [12].

$$min\ E[u] = \int_\Omega |\nabla u|\, dx\, dy + \frac{\lambda}{2} \int_\Omega (u - u_0)^2 dx dy \quad (8)$$

where, $|\nabla u|$ is the point distance between two pixels which can be obtained using the Euclidean distance, Ω represents the processed area. With the help of the Euler-Lagrange equation, the following equation is obtained.

$$\nabla . \frac{\nabla u}{|\nabla u|} - \lambda(u - u_0) = 0 \quad (9)$$

parameter λ states the coefficient level of the initial input data (noised image), which can be formulated by the following equation.

$$\lambda = \frac{1}{\sigma^2} \frac{1}{|\Omega|} \sum_{\alpha \in \Omega} \sum_{\beta \sim \alpha} w_{\alpha\beta} (u_\beta - u_\alpha)(u_a - u_\alpha^0) \quad (10)$$

where, parameter σ is the value of variance.

6. Anisotropic Diffusion Filtering

This filter method is a non-linear filtering. This diffusion equation is a partial differential equation (PDE). Anisotropic diffusion filter is obtained by the following equation [13].

$$\frac{\partial I}{\partial t} = div(c \nabla \mathrm{I}) = c.div(\nabla I) + \nabla c. \nabla I \quad (11)$$

where, g is the intensity of the image at positions x y and on the t-th iteration, so it can be denoted as $I(x, y; t)$. While I is the ultrasound image. The parameter c is the diffusion coefficient, which is defined in the following equation.

$$c(\|\nabla I\|) = \frac{1}{1 + \left(\frac{\|\nabla I\|}{k}\right)^2} \quad (12)$$

where, k is the threshold gradient parameter, and $\|\nabla I\|$ Ultrasound image gradient value.

7. Gaussian Filter

Gaussian filter is used to blur images and also to remove noise. This filter uses convolution operations and kernel matrices to reduce image noise. Gaussian kernel coefficients from the 2D Gaussian function is [14]:

$$G(x, y) = e^{\frac{x^2 + y^2}{2\sigma^2}} \quad (13)$$

where σ is the standard deviation of the distribution.

8. Wavelet Filter

Wavelet is a family of functions $f(x)$ that generated by wavelet transformation basis $\psi(x)$. This is commonly known as the *mother wavelet*. The wavelet equation can be formulated as follows [13].

$$F_W(a, b) = \int_{-\infty}^{\infty} f(x) \psi \left(\frac{x - b}{a}\right) dx \quad (14)$$

where, $a, b \in R; a \neq 0\ and\ R\ is\ real\ number$, a is the scaling or dilation parameter, b is the shift in position or translation on the x axis.

C. Segmentation using unet-cnn model

Deep vein thrombosis segmentation using Convolutional Neural Network (CNN) with U-Net architecture is effective [3], [4], [15]. This is even effective with limited image data sets. This architectural presentation is realized through biomedical image analysis [16]. The architecture diagram of U-Net CNN can be seen in Figure 2.

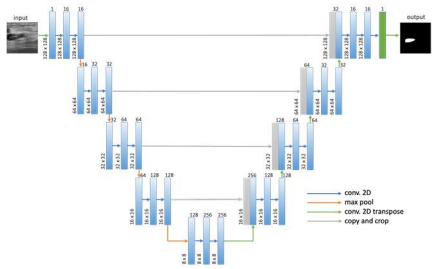

Fig. 2. Arsitektur *Unet-CNN*

D. Segmentation Performance Metrics

In this study, performance measurement for ultrasound image segmentation used two approaches: Intersection over Union (IoU) and Hausdorff distance. These evaluation metrics are commonly used to measure the accuracy of image-based detection models.

1. Intersection over Union

Intersection over union is used to measure the similarity between two 2D objects in an image [17]. IoU is used to measure the overlapping area between the masking predicted image (Y) and the ground-truth image (X). Then, it is divided by the area of union between them [18], that is:

$$IoU = \frac{area\ of\ overlap}{area\ of\ union} = \frac{|\mathrm{X} \cap \mathrm{Y}|}{|\mathrm{X} \cup \mathrm{Y}|} \quad (15)$$

$$IoU\ (X, Y) = \frac{\sum_{i=1}^{n} \min(X_i, Y_i)}{\sum_{i=1}^{n} \max(X_i, Y_i)} \quad (16)$$

where: $$X_i, Y_i \in \{0,1\}, \forall i \in \{1, n\} \quad (17)$$

IoU results can be in the range of values from 0 to 1. This can also be converted into percentage form. Prediction results were obtained with an IoU score close to 1, then the results of the segmentation model have the predictive ability with results closer to ground-truth.

2. Hausdorff Distance

Hausdorff distance measures segmentation performance by calculating the distance between two-point set images. In this study, the Hausdorff distance was used to compare the ground-truth image with the predicted image based on the results of ultrasound image segmentation. Hausdorff distance will be 0, if there is a similarity between two image objects. on the other hand, the Hausdorff distance will be of high value if the similarity between the two-point sets is getting further away. [19]. Moreover, measurement of segmentation performance using Hausdorff distance is often used in medical image segmentation [20]. Hausdorff distance calculates the difference in length from each edge of the image, using the following formula:

$$hd(\mathrm{A},\mathrm{B}) = max_{i,j}\{d(\mathrm{A}_i,\mathrm{B}),d(\mathrm{B}_j,\mathrm{A})\} \quad (18)$$

where,

$$d(\mathrm{A}_i,\mathrm{B}) = min_k\{d(\mathrm{A}_i,\mathrm{B}_k)\} \quad (19)$$

$$d(\mathrm{B}_j,\mathrm{A}) = min_k\{d(\mathrm{B}_j,\mathrm{A}_k)\} \quad (20)$$

Distance $d(\mathrm{A}_i,\mathrm{B})$ is a metric obtained by calculating the distance, i.e. the Euclidean distance, at pixel A_i to the nearest edge pixel of B. This applies vice versa for distance measurements on $d(\mathrm{B}_j,\mathrm{A})$ [21].

III. Experiment Result And Discussion

In this research, three main processes was proposed, and the first process was the denoising filter. These filters are often used in medical image processing. The denoising filters used in this research are Wiener filter, Lee filter, Non-local mean filter, Median filter, Total variation filter, Anisotropic diffusion filter, Gaussian filter, and Wavelet filter. This process serves to reduce the speckle noise presented in the ultrasound image. Thus, this will result in better segmentation performance. The second process was ultrasound image segmentation. This process aims to segment the symptoms of deep vein thrombosis on ultrasound images. This process uses a deep learning method with the U-Net CNN architecture. The third process was measuring the performance of deep vein thrombosis segmentation. This process aims to determine the accuracy of segmentation using the U-Net CNN architecture. The testing system in this study uses a deep vein thrombosis dataset that has been given a mask. Labeling of images was done manually by a professional medical team.

In the training process, the U-Net CNN model uses python 3 with the Spyder version 5 and runs on a personal computer with specifications: Intel Xeon E3-1240 v5 (3.5 GHz), 16 GB DDR4 2133MHz, Nvidia Quadro 2 GB, and NVMe SSD 250GB.

A. Denoising filters

There are eight denoising filter algorithms used in this study. Raw image data used one sample of ultrasound images with suspected symptoms of deep vein thrombosis. The results of the filter process can be seen in Figure 3.

B. Segmentation DVT ultrasound image

The segmentation process used U-Net CNN. The input data was a filtered ultrasound image, which used a denoising filter. As for the U-Net CNN configuration using parameters including:

- Optimizer=Adam with learning rate (lr), that has a value of 1e-3;
- loss = binary_crossentropy;
- metrics = MeanIoU
- epochs = 50
- early stopping with patience = 2, and monitor = val_loss

The training and validation process using U-Net CNN based on a denoising filter was run several times to get the average performance result. Each filter was tested for 10 times. The dataset used in this study was divided into two parts. The first part was the training data with the amount of data 80% of the entire dataset. Meanwhile, for data testing, the data was 20% of the dataset. The training and validation data selection was obtained randomly from the dataset. The results of the average performance of the proposed model in this study can be seen in Table 1.

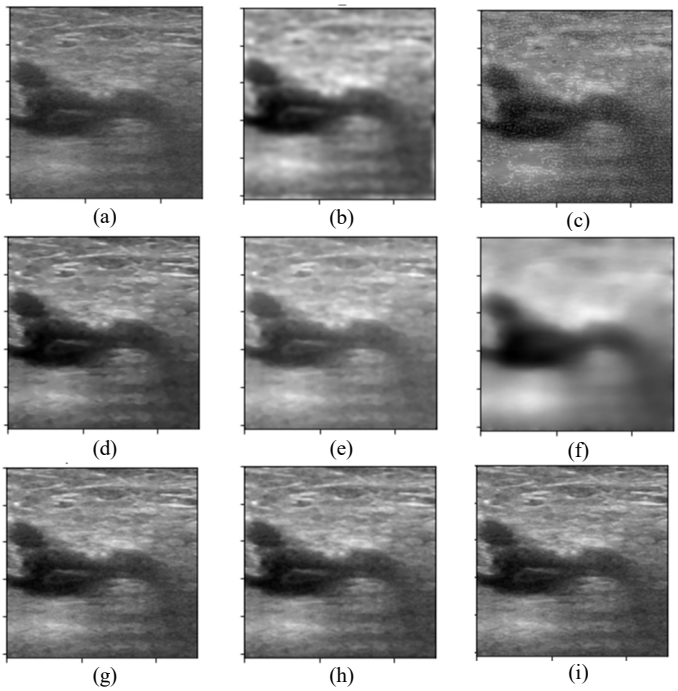

Fig. 3. Denosing filter example results. (a) Original image, (b) Wiener filtering, (c) Lee Filtering, (d) Non-local means Filtering, (e) Median filtering, (f) Total variation filter, (g) Anisotropic diffusion, (h) Gaussian filtering, and (i) Wavelet filter.

The performance of U-Net CNN based on a denoising filter can be seen in Table 1. The accuracy and loss parameters indicate the version of the segmentation model using U-Net CNN. Meanwhile, the mean IoU and mean Hausdorff distance parameters indicate how similar the segmentation results are to the expected object. U-Net CNN segmentation using the wiener

filter has an accuracy value of 99.02 %. This filter has the best deal based on the segmentation model than other filters. Meanwhile, based on the loss parameter for the U-Net CNN model, the median filter has the best value, with a value of 0.025.

TABLE I. SEGMENTATION USING DENOISING FILTERS PERFORMANCE

Unet Segmentation using Denoising Filter	*Accuracy*	*loss*	*Mean IoU*	*Mean hausdorff*
Non-filter	98.70 %	0.0311	80.52%	4.84
wiener	**99.02** %	0.0268	82.86%	4.33
lee	98.27 %	0.0474	73.54%	5.80
Non-local means	98.83 %	0.0290	83.04%	4.34
Median	98.97 %	**0.0250**	83.32%	4.28
Total variation	98.80 %	0.0361	80.58%	4.71
Anisotropic diffusion	98.29 %	0.0401	78.39%	5.07
Gaussian	99.00 %	0.0252	**84.90**%	**4.17**
Wavelet	98.88 %	0.0265	83.86%	4.33

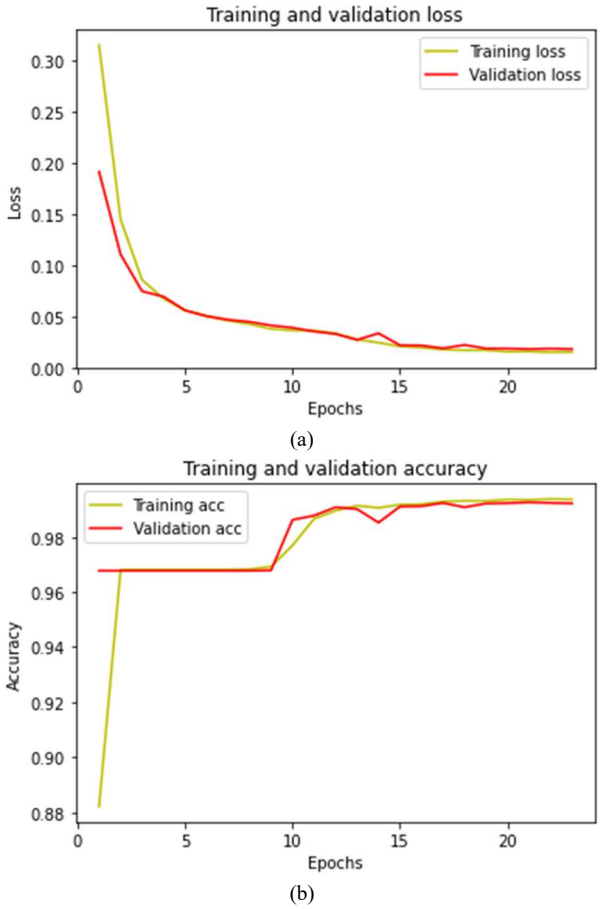

Fig. 4. Training and validation unet-cnn model based on gaussian filter. (a) loss parameter, (b) accuracy parameter.

Fig. 5. Segmentation DVT result using unet-cnn model based on gaussian filter. (a) image test, (b) ground truth image, (c) predicted image.

In this study, the performance measurement of segmentation results uses two measurement models. The measurement models are the Intersection over Union (IoU) model and the Hausdorff distance model. Based on the results of the running test as shown in Table 1, the gaussian filter has the best results based on the IoU and Hausdorff distance measurements. This means that the prediction results of DVT image segmentation using U-Net CNN with gaussian filter get an accuracy of 84.90% based on IoU measurements. Meanwhile, the gaussian filter got the best performance in the performance test using the Hausdorff distance, which was 4.17. Measures based on the Hausdorff distance will result in 0 if two objects have perfect similarities. Thus, the smaller the Hausdorff value, the closer the difference between the predicted and expected results will be. Therefore, the Gaussian filter is the best filter for denoising filter in segmentation using U-Net CNN for DVT ultrasound image.

Then, segmentation was performed using a Gaussian denoising filter on ultrasound images of deep vein thrombosis to determine the area of DVT symptoms. The training and validation process at U-Net CNN using a gaussian filter can be seen in Figure 4. The training and validation process stops at the 23rd epoch with a validation loss value of 0.018, while the validation accuracy is at a value of 99.22%.

U-Net CNN is used to segment areas with symptoms of deep vein thrombosis. The result of segmentation using U-Net CNN is the image prediction of the symptom area. This is to evaluate risk factors by looking at the area of deep vein thrombosis. So this is important for the accuracy of predictions. If the prediction performance is less accurate, it will produce less precise predictions. This will lead to overestimate or underestimate the symptoms of DVT. DVT Segmentation using U-Net CNN model based on gaussian filter can be seen in Figure 5.

In this study, the measurement of the performance area of the prediction area uses the object difference between the prediction masking image and the ground-truth image. Prediction masking image can be denoted by Y variable, while the ground-truth image can be indicated by X variable. Thus, the difference between predicted object and Ground-Truth image can be denoted by $Y - X = \{x | x \in Y,\ x \notin X\}$. Image variables X and Y in the binary case. This measurement will produce a value of 0. There is no difference in the prediction masking image and the ground-truth image. If a ground truth object had no associated predicted object, then this indicates that the segmentation prediction results underestimate the DVT symptom. This equation can be defined in equation (21). Meanwhile, a predicted object had no associated ground truth object, which shows that the picture of DVT symptoms appeared beyond expectations. So, this is called an overestimate. This equation can be defined in equation (22).

$$UnderEstimate\ (X,Y) = \frac{\sum_{i=1}^{n}(X_i > Y_i)}{\sum_{i=1}^{n}(X_i)} \tag{21}$$

$$OverEstimate\ (X,Y) = \frac{\sum_{i=1}^{n}(X_i < Y_i)}{\sum_{i=1}^{n}(X_i)} \tag{22}$$

where $X_i, Y_i \in \{0,1\}, \forall i \in \{1,n\}$

Based on the calculation of the segmentation prediction error using equation 21, the result is 0.6%. This shows that, the area

of a ground truth is almost entirely covered by the masking image prediction results. While the calculation of the area masking image prediction error area that is not expected is 52.98%. Thus, this prediction results in an overestimation of the suspicion of deep vein thrombosis.

IV. Conclusion

This study proposes a model for segmenting ultrasound images of deep vein thrombosis using U-Net CNN based on a denoising filter and then calculating the area suspected to be a symptom of deep vein thrombosis predicted using U-Net CNN. The denoising filters used in this research are wiener filters, lee filters, non-local means filters, median filters, total variation filters, anisotropic diffusion filters, Gaussian filters, and Wavelet filters. The dataset was captured and recorded using an ultrasound device carried out by medical experts. The dataset was obtained from 4 patients who had symptoms of DVT. Each DVT recorded data was extracted into frames. The full frames obtained were 317 frames. Then the ultrasound image data was manually labeled by medical personnel. The experimental results show that the Gaussian filter has the best results: an average accuracy of 99%, an average loss parameter of 0.0252 score, a mean IoU of 84.9% accuracy, and a mean Hausdorff distance of 4.17 score. Prediction of the symptom area of deep vein thrombosis using U-Net CNN with a gaussian filter resulted in the number of predicted areas that matched the mask area of 99.4%, while the number of areas that were in the underestimate category was 0.6% and overestimated was 52.98%. We would like to investigate detection and classification of DVT models for further research.

Acknowledgment

This study has been funded by Beasiswa Pendidikan Indonesia (BPI) from Kementerian Pendidikan, Kebudayaan, Riset, dan Teknologi (Kemdikbudristek) and Lembaga Pengelola Dana Pendidikan (LPDP), Indonesia.

References

[1] M. G. Beckman, W. C. Hooper, S. E. Critchley, and T. L. Ortel, "Venous Thromboembolism. A Public Health Concern," *Am. J. Prev. Med.*, vol. 38, no. 4 SUPPL., pp. S495–S501, 2010, doi: 10.1016/j.amepre.2009.12.017.

[2] L. Zhao *et al.*, "Measurement of thrombus resolution using three-dimensional ultrasound assessment of deep vein thrombosis volume," *J. Vasc. Surg. Venous Lymphat. Disord.*, vol. 2, no. 2, pp. 140–147, 2014, doi: 10.1016/j.jvsv.2013.08.009.

[3] C. Huang *et al.*, "Fully Automated Segmentation of Lower Extremity Deep Vein Thrombosis Using Convolutional Neural Network," *Biomed Res. Int.*, vol. 2019, 2019, doi: 10.1155/2019/3401683.

[4] B. Kainz *et al.*, "Non-invasive diagnosis of deep vein thrombosis from ultrasound imaging with machine learning," *npj Digit. Med.*, vol. 4, no. 1, pp. 1–18, 2021, doi: 10.1038/s41746-021-00503-7.

[5] F. Mohamed and C. Vei Siang, "A Survey on 3D Ultrasound Reconstruction Techniques," *Artif. Intell. - Appl. Med. Biol.*, 2019, doi: 10.5772/intechopen.81628.

[6] I. M. G. Sunarya, E. M. Yuniarno, T. A. Sardjono, I. Sunu, P. M. A. van Ooijen, and I. K. E. Purnama, "3D reconstruction of carotid artery in B-mode ultrasound image using modified template matching based on ellipse feature," *Comput. Methods Biomech. Biomed. Eng. Imaging Vis.*, vol. 8, no. 3, pp. 301–312, 2020, doi: 10.1080/21681163.2019.1692235.

[7] Z. Hosseini and M. H. Bibalan, "Speckle noise reduction of ultrasound images based on neighbor pixels averaging," in *2018 25th Iranian Conference on Biomedical Engineering and 2018 3rd International Iranian Conference on Biomedical Engineering, ICBME 2018*, 2018, pp. 1–6, doi: 10.1109/ICBME.2018.8703576.

[8] B. H. S. Asli *et al.*, "Ultrasound Image Filtering and Reconstruction Using DCT/IDCT Filter Structure," *IEEE Access*, vol. 8, pp. 141342–141357, 2020, doi: 10.1109/ACCESS.2020.3011970.

[9] A. S. Pramulen, E. M. Yuniarno, J. Nugroho, I. M. G. Sunarya, and I. K. E. Purnama, "Carotid Artery Segmentation on Ultrasound Image using Deep Learning based on Non-Local Means-based Speckle Filtering," *CENIM 2020 - Proceeding Int. Conf. Comput. Eng. Network, Intell. Multimed. 2020*, pp. 360–365, 2020, doi: 10.1109/CENIM51130.2020.9298009.

[10] P. Coupé, P. Hellier, C. Kervrann, and C. Barillot, "Nonlocal means-based speckle filtering for ultrasound images," *IEEE Trans. Image Process.*, vol. 18, no. 10, pp. 2221–2229, 2009, doi: 10.1109/TIP.2009.2024064.

[11] O. V. Michailovich and A. Tannenbaum, "Despeckling of medical ultrasound images," *IEEE Trans. Ultrason. Ferroelectr. Freq. Control*, vol. 53, no. 1, pp. 64–78, 2006, doi: 10.1109/TUFFC.2006.1588392.

[12] S. Huang and S. Wan, "A Total Variation Denoising Method Based on Median Filter and Phase Consistency," *Sens. Imaging*, vol. 21, no. 1, pp. 1–15, 2020, doi: 10.1007/s11220-020-00281-8.

[13] S. H. Contreras Ortiz, T. Chiu, and M. D. Fox, "Ultrasound image enhancement: A review," *Biomed. Signal Process. Control*, vol. 7, no. 5, pp. 419–428, 2012, doi: 10.1016/j.bspc.2012.02.002.

[14] M. Wang, S. Zheng, X. Li, and X. Qin, "A new image denoising method based on Gaussian filter," *Proc. - 2014 Int. Conf. Inf. Sci. Electron. Electr. Eng. ISEEE 2014*, vol. 1, pp. 163–167, 2014, doi: 10.1109/InfoSEEE.2014.6948089.

[15] R. Tanno *et al.*, *AutoDVT: Joint real-time classification for vein compressibility analysis in deep vein thrombosis ultrasound diagnostics*, vol. 11071 LNCS. Springer International Publishing, 2018.

[16] O. Ronneberger, P. Fischer, and T. Brox, "U-NET: Convolutional Networks for Biomedical Image Segmentation," *Int. Conf. Med. Image Comput. Comput. Interv.*, vol. 9351, no. Cvd, pp. 12–20, 2015, doi: 10.1007/978-3-319-24574-4.

[17] H. Rezatofighi, N. Tsoi, J. Gwak, A. Sadeghian, I. Reid, and S. Savarese, "Generalized intersection over union: A metric and a loss for bounding box regression," *Proc. IEEE Comput. Soc. Conf. Comput. Vis. Pattern Recognit.*, vol. 2019-June, pp. 658–666, 2019, doi: 10.1109/CVPR.2019.00075.

[18] R. Padilla, S. L. Netto, and E. A. B. Da Silva, "A Survey on Performance Metrics for Object-Detection Algorithms," *Int. Conf. Syst. Signals, Image Process.*, vol. 2020-July, pp. 237–242, 2020, doi: 10.1109/IWSSIP48289.2020.9145130.

[19] A. A. Taha and A. Hanbury, "An Efficient Algorithm for Calculating the Exact Hausdorff Distance," *IEEE Trans. Pattern Anal. Mach. Intell.*, vol. 37, no. 11, pp. 2153–2163, 2015, doi: 10.1109/TPAMI.2015.2408351.

[20] D. Karimi and S. E. Salcudean, "Reducing the Hausdorff Distance in Medical Image Segmentation with Convolutional Neural Networks," *IEEE Trans. Med. Imaging*, vol. 39, no. 2, pp. 499–513, 2020, doi: 10.1109/TMI.2019.2930068.

[21] C. H. T. Yang, S. H. Lai, and L. W. Chang, "Reliable image matching via modified Hausdorff distance with normalized gradient consistency measure," *ITRE 2005 - 3rd Int. Conf. Inf. Technol. Res. Educ. - Proc.*, vol. 2005, pp. 158–161, 2005, doi: 10.1109/ITRE.2005.1503090.